Progress In Electromagnetics Research Letters, Vol. 62, 41–47, 2016

Metal-Frame GPS Antenna for Smartwatch Applications

Saou-Wen Su* and Cheng-Tse Lee

Abstract—The integration of a loop antenna into the top metal frame of a smartwatch wearable device is introduced. The loop antenna was made of a 1-mm thick, rectangular metal frame, which was stacked 1.5 mm above the lower metal frame of the watch having a size of 7 mm × 35 mm × 40 mm. The system circuit board was encircled by the lower, rectangular metal frame with a 1 mm gap between the perimeter of the ground plane and the metal frame. The top metal frame was fed in a corner on the frame's longer edge with two shorting portions short-circuited to the system ground. By carefully positioning the two shorting for the top metal frame, the proposed loop antenna can provide the global positioning system (GPS) operation at 1575 MHz for smartwatch applications.

1. INTRODUCTION

Currently smartwatch wearable devices are receiving more and more attention as the devices provide add-on, intelligent functions and serve as a companion to the mobile phones. The majority of smartwatches receive/transmit the real-time information, such as time, messages, and even voice calls from/to the phones via Bluetooth with the built-in, 2.4 GHz antennas within the watches [1–3]. Many smartwatches also allow users to record various fitness activities such as walking, running, cycling and many others. For smartwatches with the global positioning system (GPS) connectivity, the standalone mode on the watch is able to store all the metrics from the exercise sessions without the need of the companion phone when running/cycling. Very few GPS enabled smartwatches are available on the market, which has created a gap in the associated literature concerned with smartwatch antenna design. This motivates us to propose a feasible and new design to implement a GPS antenna that is fully integrated with the metal frame of the smartwatch device.

In this Letter, the overall size of the design, including the top and lower rectangular metal frames of the smartwatch, measures 7 mm × 35 mm ×40 mm, which can practically accommodate a 1.45 ∼ 1.65 inch display. The antenna was integrated into the top metal frame, which was stacked 1.5 mm above the lower metal frame. The antenna was fed in the corner of the watch with one shorting close to the feed port and the other shorting located at about half wavelength at 1575 MHz from the feeding (see Fig. 1). The two shorting portions were short-circuited to the ground of the system circuit board, which was encircled by the lower metal frame with a 1 mm gap between the perimeter of the ground and the frame. The design in this paper uses the linearly-polarized (LP) antennas [4–6], which are widely used in mobile devices for GPS signal reception. Also, the antenna design is of a loop type but substantially different from the conventional one-feeding, one-shorting loop structure [7–10]. The results showed that a smaller, half-wavelength loop size was obtained with the use of the extra short-circuiting close to the antenna feeding. The effects of the user's forearm/hand phantom, particularly the wrist part, on the return loss and the radiation performance were also studied. Details of a preferred design prototype and the operating principle thereof are described and discussed in the article.

Received 30 May 2016, Accepted 26 August 2016, Scheduled 9 September 2016

* Corresponding author: Saou-Wen Su (Saou-Wen_Su@asus.com).
The authors are with the Antenna Design Office, Advanced EM & Wireless Communication R&D Center, ASUS, Taipei 11259, Taiwan.

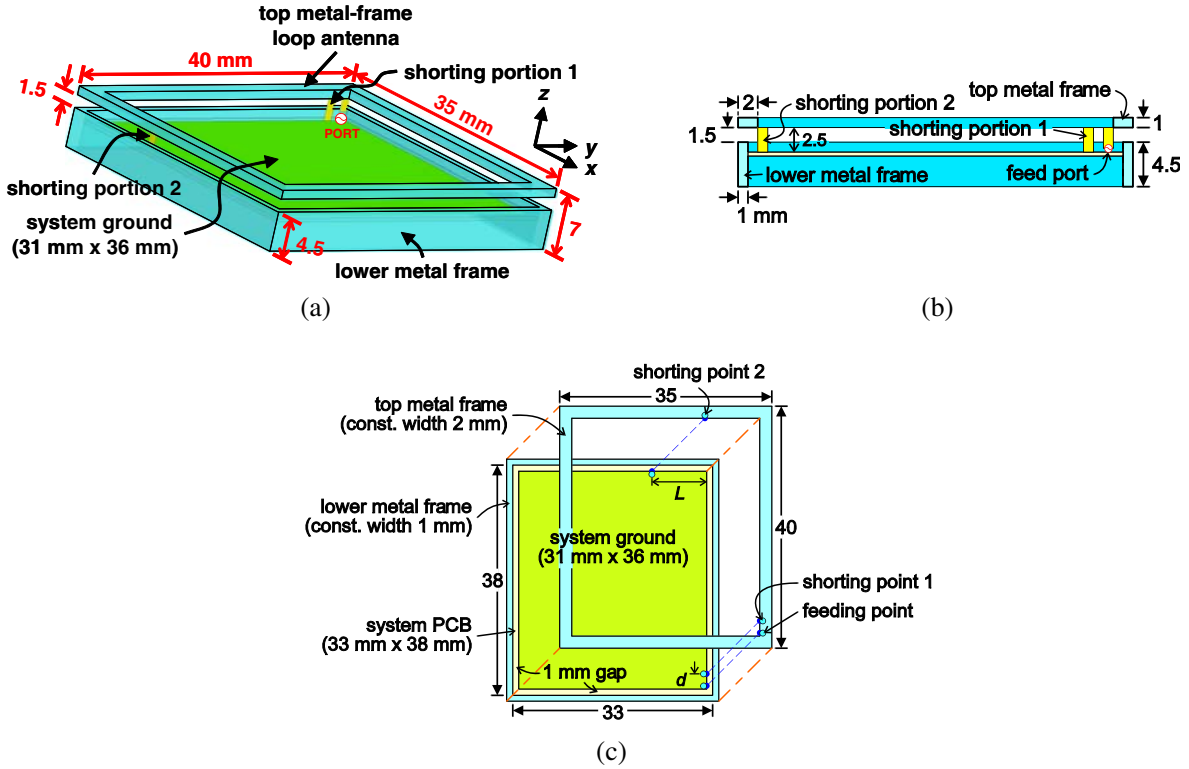

Figure 1. (a) Perspective drawing of the proposed GPS loop antenna integrated into the top metal frame of a smartwatch. (b) Sectional view of the top metal frame, the lower metal frame, and the system PCB. (c) Top view of the proposed design.

2. PROPOSED METAL-FRAME ANTENNA

Figure 1(a) demonstrates the configuration of the proposed loop antenna integrated into the top metal frame of a smartwatch. The overall size of the design, including the top and lower metal frames, measures 7 mm ×35 mm ×40 mm. The top-frame loop antenna was 1 mm in thickness and stacked 1.5 mm above the lower metal frame (also 1 mm thick). The loop was fed in the corner of the watch frame with two shorting portions of 2.5 mm in height, short-circuited to the system ground of size 31 mm ×36 mm, which was encircled by the said lower frame and separated by a 1 mm gap. The 1-mm separation was designed to avoid the contact between the lower frame and the system ground. The cross-sectional view of the design is shown in Fig. 1(b) for reference. In this case, the metal-frame antenna is placed 2.5 mm above the system printed circuit board (PCB). Note that if the grounding of the lower frame to the system ground is necessary for the electrostatic discharge (ESD) design, a grounding portion protruding either from the frame or the system ground can be employed as long it is located between the two shorting portions, on which relatively weak surface currents (see contour portion of A, D, E, H in Fig. 4) are excited. The results for the said additional grounding were studied but not shown in this paper for brevity.

The exploded-view drawing with detailed dimensions for the antenna is shown in Fig. 1(c). The top frame antenna has a constant width of 2 mm, and its projection area covers the thickness (1 mm) of the lower frame and the no-ground portion (1 mm gap between the lower frame and the ground) on the system PCB. The feeding point of the antenna and the first shorting point (point 1) were first fixed in the corner of the top metal frame on the longer edge (length 40 mm). The second shorting point (point 2) was then found on the shorter edge (length 35 mm) with a distance L to the corner where the said two edges intersect. Note that the distance d of shorting portion 1 to the feed port was initially fixed in the range of 0.5 mm to 3 mm for smaller PCB layout as preferred. Then, the location L of shorting

portion 2 basically controlled the desired antenna frequencies. By carefully positioning the two shorting with one very close to the feeding and the other with suitable resonant length from the feeding, the proposed loop antenna is able to generate a well-matched half-wavelength mode covering the GPS band at 1575 MHz. The effects of the distance d of shorting portion 1 to the feed port and the location L of shorting portion 2 on the antenna frequencies will be discussed with the aid of Fig. 6 in Section 3. Note that when there was no shorting portion 1 (no shorting next to the feeding), the operating frequencies would increase to about 1925 MHz with poor antenna matching (data not shown for brevity). This resonant mode showed similar surface-current properties to those studied in Fig. 4. This also suggests that compared with the conventional one-feeding, one-shorting loop structure [7–10], the use of the extra short-circuiting next to the feed port allows the proposed antenna to obtain a smaller antenna size. For the antenna measurement, a 50-Ω mini-coaxial cable with a miniature coaxial connector was utilized with the inner conductor soldered at the feeding point and the outer shielding connected to the system ground (see photo in Fig. 2). Note that for mass production, the feeding and shorting portions can be replaced by the surface-mount technology (SMT) spring.

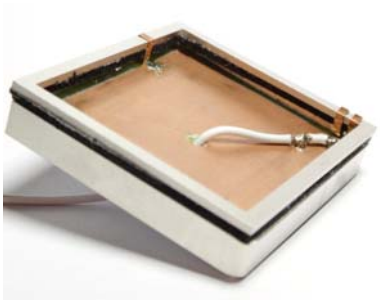

Figure 2. Photo of a constructed prototype fed by a 50-Ω mini-coaxial cable.

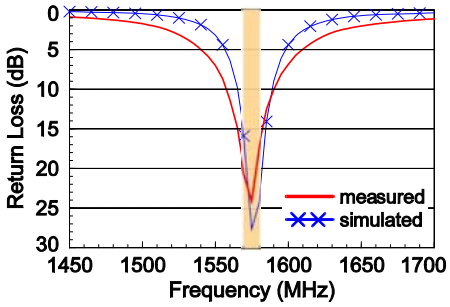

Figure 3. Measured and simulated return losses for the prototype: $d = 1$ mm, $L = 8.5$ mm.

3. RESULTS AND DISCUSSION

Figure 3 shows the measured and simulated return losses of a design prototype. The experimental data generally agree with the simulation results, which is based on the finite element method using the high frequency structure simulator (HFSS) version 11 [11]. The measured impedance bandwidth, defined by 10-dB return loss, covers the frequencies ranging between 1560 MHz and 1590 MHz, which easily meet the required bandwidth for GPS operation. The simulated, surface-current distributions for the antenna excited at 1575 MHz are shown in Fig. 4. To identify the current nulls, the currents are illustrated in the form of vectors (arrow shape) with the nulls denoted as cross in the figure. It is first seen that relatively large currents are distributed along the path A, B, C, D on the top metal frame and the corresponding path E, F, G, H, right below the top frame, on the system ground. Together with the feed port and the shorting portion (DE), the current paths form a close loop structure, which produces two current nulls, respectively, on the top metal frame and the system ground. The two current nulls on the paths B, C and F, G are also occurred in close proximity. Other portions along the contour of A, D, E, H are populated with much weaker currents. These properties infer that part of the antenna resonance path is merged into the ground plane. For the proposed design, the top metal frame can be considered a half-wavelength loop radiator while that in combination with the image current on the ground exhibit a one-wavelength loop mode.

The proposed design can also be fed in the middle of the frame's longer edge. Fig. 5(a) illustrates the simulated return losses for the proposed antenna and the reference case (signal feeding located in the middle of the top frame) with the surface currents of the reference antenna shown in Fig. 5(b). First, the obtainable impedance bandwidth is similar for the two antennas, and the distance between shorting portion 1 and the feed port remains the same ($d = 1$ mm in these cases). This behavior suggests that the design provides flexibility for the antenna feeding placement on the system PCB, which relaxes the system-level integration inside the small electronic device like smartwatches. The two current nulls in

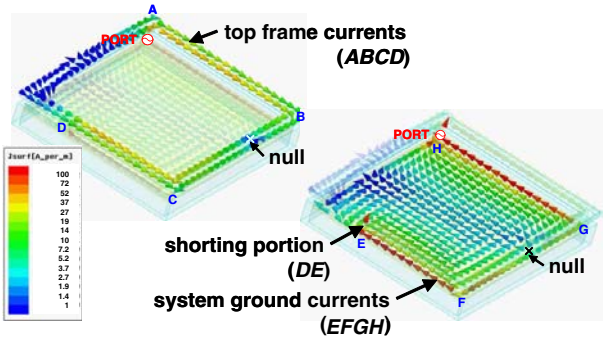

Figure 4. Simulated surface currents in the form of vectors at 1575 MHz for the prototype studied in Fig. 3.

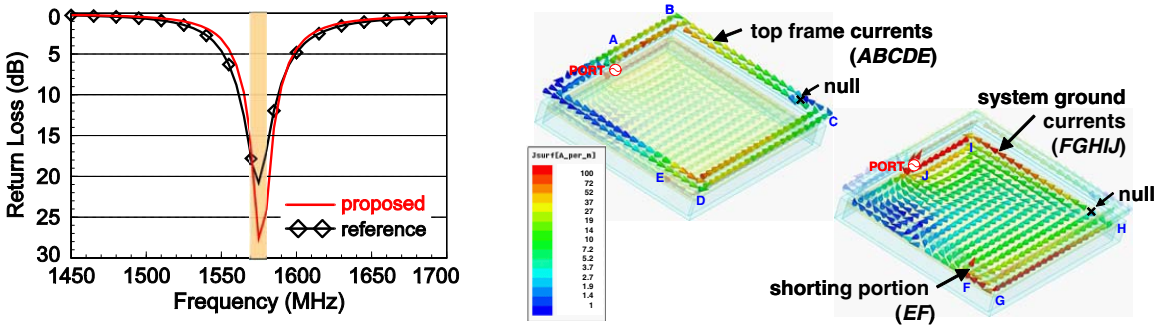

(a) (b)

Figure 5. (a) Simulated return losses for the proposed and the reference (the case with signal feeding located in the middle of the frame's longer edge; $d = 1$ mm, $L = 25$ mm) antennas. (b) Simulated surface currents for the reference antenna excited at 1575 MHz.

close proximity are also identified on the current path A, B, C, D, E on the top metal frame and the path F, G, H, I, J on the system ground, respectively. The phenomena of the surface currents for the reference antenna are substantially the same as those for the proposed prototype. Note that the operating principles are the same for both cases, and the obtained peak gains are also similar. However, the radiation patterns for the proposed in the x-z and y-z planes (see Fig. 7) become quite similar but change to the x-z and y-z planes for the reference. That is, when the signal feeding moves from the corner to the middle on the same frame edge, the radiation patterns are rotated by 90 degrees with respect to the $+z$ direction.

Figures 6(a) and 6(b) show the simulated return losses for the proposed antenna as a function of the distance d of shorting portion 1 to the feed port and the location L of shorting portion 2, respectively. It can be seen that the location for shorting portion 1 does not largely affect the impedance bandwidth but rather the input matching at the antenna resonance frequency. Therefore, once the desired impedance bandwidth has been attained, engineers can manipulate this parameter to fine-tune the antenna matching. For the location L of shorting point 2, the antenna frequencies increase with an increase in L from 7.5 mm to 9.5 mm. This is because a larger value L generates a shorter resonant path for the loop (see current paths in Fig. 4), which in turn leads to higher operating frequencies. In this study, the near optimized value for the location L at the watch shorter edge was found to be 8.5 mm, allowing the top metal-frame antenna to have the half-wavelength loop mode at 1575 MHz.

The over-the-air (OTA) performance of the design prototype in free space was studied. Fig. 7 gives the far-field, two-dimensional (2D) radiation patterns in the x-z and y-z planes at 1575 MHz. The measurement was made at the 4 m $\times$4 m $\times$4 m, SATIMO OTA chamber, which uses the conical-cut method, of SG 64 model [12]. The $+z$ direction (the direction above the display) in this design is

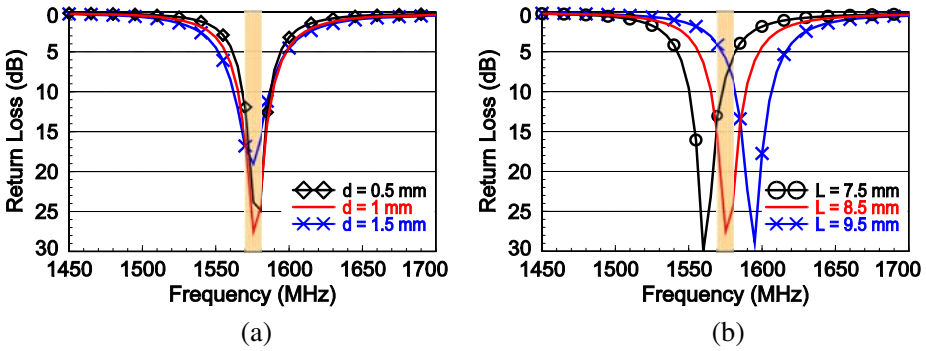

Figure 6. Simulated return losses for the proposed antenna as a function of (a) the distance d and (b) the location L of the two shorting portions; other dimensions are the same as those studied in Fig. 3.

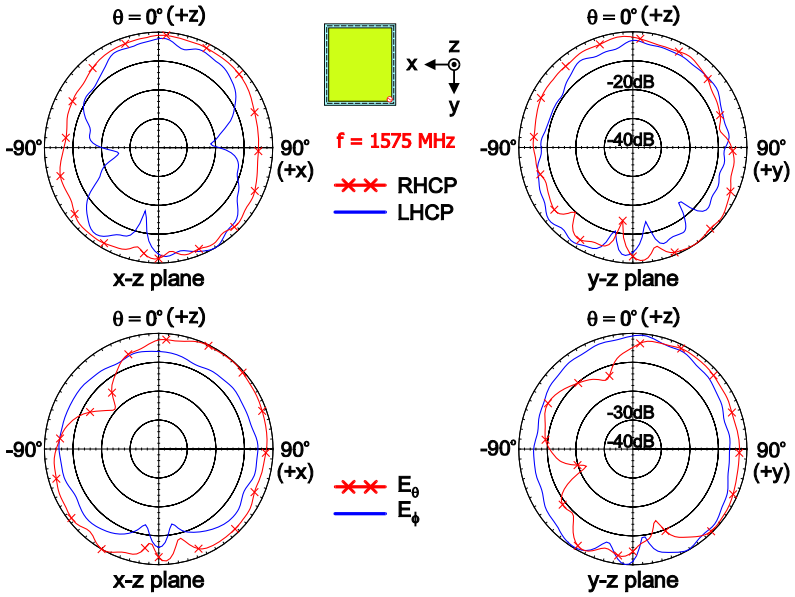

Figure 7. Measured 2-D radiation patterns at 1575 MHz for the prototype studied in Fig. 3.

the main concern for the criteria, in which the relative strength of the right-hand circular polarization (RHCP) is required to exceed that of the left-hand circular polarization (LHCP) [13]. As seen in Fig. 7, the RHCP radiation in the $+z$ direction is larger than the LHCP one. Because the proposed design utilizes the LP antenna to receive the GPS signals, the radiation patterns in E_θ and E_φ fields are also shown in the figure. Fig. 8 presents the measured, peak gain and antenna efficiency against frequency for the proposed antenna. The antenna efficiency in the frequency range of 1570 to 1580 MHz is about $41 \sim 47\%$; the peak gain is seen in the range of 1.0 to 1.4 dBi over the said frequency range. Note that the antenna efficiency was obtained by measuring the total radiated power of the antenna under test (AUT) over the three-dimensional spherical radiation and then dividing that sum by the AUT input power of 0 dBm, in which the antenna impedance mismatch losses are taken into account, and the realized gain [14] and the antenna efficiency [15] were measured.

Finally, the design was also tested with the user's forearm/hand phantom using CTIA [16] compliant RF phantom by the SPEAG [17], which is widely known for their dosimetric assessment system (DASY). The anthropomorphically shaped forearm-hand phantom is very beneficial for the OTA evaluations of wrist-worn smartwatch devices because it is not ethical to conduct the radiation measurement with a human being wearing/holding the AUT in the anechoic chamber. In this study, the prototype was placed on the wrist of the phantom with an air gap of 3 mm, which represents the distance between

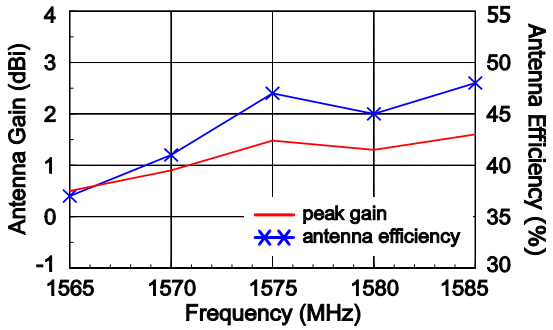

Figure 8. Measured antenna gain and efficiency for the antenna studied in Fig. 3.

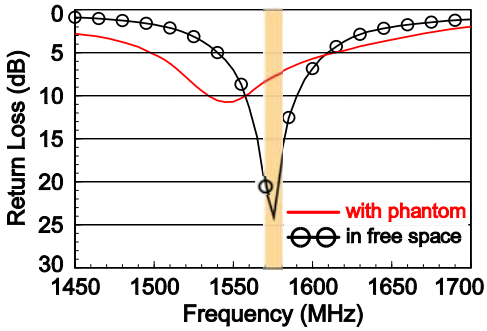

Figure 9. Measured return losses for the proposed design with the user's forearm and hand phantom and for the antenna in free space.

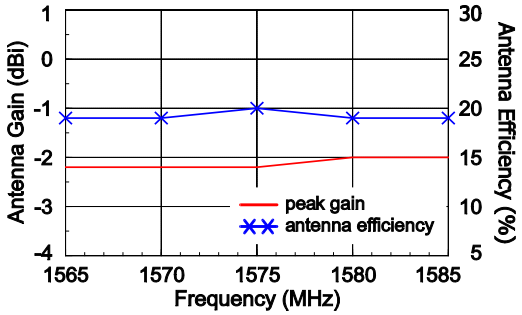

Figure 10. Measured antenna gain and efficiency for the antenna with the user's forearm and hand phantom studied in Fig. 9.

the lower metal frame and the wrist when a smartwatch back cover is included [2]. With the presence of the forearm and the hand, it is seen that in Fig. 9, the antenna frequencies are detuned toward the lower frequencies around 1550 MHz with the impedance matching still better than 7.3-dB return loss, compared with the design in free space. As for the peak gain and antenna efficiency, the measured results in Fig. 10 show that the gain and efficiency are decreased by 3.6 dBi and 3.9 dB, respectively. In general, the antenna efficiency deteriorates with every millimeter decrease of the gap between the wearable-device antenna and the skin [18].

4. CONCLUSION

A novel design incorporating the loop antenna into the smartwatch metal frame for GPS operation has been presented. The GPS antenna was integrated into the top metal frame above the watch lower metal frame and utilized the system ground, which was encircled by the said lower frame, as part of the loop resonant path. With one shorting arranged next to the feed port and the other one properly located, the half-wavelength loop mode with good impedance bandwidth was attained. In addition, the use of the two short-circuiting also made the proposed antenna obtain a smaller loop size. The antenna can be fed in the corner of the top metal frame or in the middle of the frame's longer edge with similar antenna performance obtained. The antenna design was also tested with the user's forearm/hand phantom. Results showed that the input matching was degraded but still better than about 7.3-dB return loss; the peak gain and antenna efficiency were decreased by 3.6 dBi and 3.9 dB, respectively, absorbed by the lossy medium of the forearm/hand phantom. Therefore, for the system level design with respect to the GPS-chip sensitivity and battery life, the user's hand effects on the smartwatch antenna are better taken into account.

REFERENCES

1. Chen, Y. S. and T. Y. Ku, "A low-profile wearable antenna using a miniature high impedance surface for smartwatch applications," *IEEE Wireless Antennas Propagat. Lett.*, Vol. 15, 1144–1147, 2016.
2. Su, S. W. and Y. T. Hsieh, "Integrated metal-frame antenna for smartwatch wearable device," *IEEE Trans. Antennas Propagat.*, Vol. 63, 3301–3305, 2015.
3. Wu, D., S. W. Cheung, Q. L. Li, and T. I. Yuk, "Slot antenna for all-metal smartwatch applications," *European Conf. Antennas Propagat.*, 1144–1147, Davos, Switzerland, 2016.
4. Ahn, J., S. Kim, M. J. Lee, A. S. Kim, and Y. Kim, "Small global positioning system antennas on a printed circuit board for mobile handsets loaded with lumped elements," *Microwave Opt. Technol. Lett.*, Vol. 55, 576–580, 2013.
5. Su, S. W., "Linearly-polarized patch PIFA for GPS/GLONASS operation for tablet-computer applications," *Microwave Opt. Technol. Lett.*, Vol. 57, 149–153, 2015.
6. Wong, K. L., Z. G. Liao, and W. Y. Li, "Hybrid loop/monopole antenna with a passive bandstop circuit for the LTE/GPS operation in the tablet computer," *Microwave Opt. Technol. Lett.*, Vol. 58, 630–635, 2016.
7. Su, S. W., "Concurrent dual-band six-loop-antenna system with wide 3-dB beamwidth radiation for MIMO access points," *Microwave Opt. Technol. Lett.*, Vol. 52, 1253–1258, 2010.
8. Su, S. W., "High-gain dual-loop antennas for MIMO access points in the 2.4/5.2/5.8 GHz bands," *IEEE Trans. Antennas Propagat.*, Vol. 58, 2412–2419, 2010.
9. Su, S. W., "Integration of loop and slot antennas into one-piece metal plate for concurrent 2.4- and 5-GHz wireless local area network operation," *Microwave Opt. Technol. Lett.*, Vol. 54, 815–820, 2012.
10. Su, S. W., "Compact four-loop-antenna system for concurrent, 2.4- and 5-GHz WLAN operation," *Microwave Opt. Technol. Lett.*, Vol. 56, 208–215, 2014.
11. ANSYS HFSS, ANSYS Inc., http://www.ansys.com/Products/Electronics/ANSYS-HFSS.
12. SG 64, SATIMO, http://www.satimo.com/content/products/sg-64.
13. Wang, J. H., "Antennas for global navigation satellite system (GNSS)," *Proc. IEEE*, Vol. 100, 2349–2355, 2012.
14. Volakis, J. L., *Antenna Engineering Handbook*, 4th Edition, Chapter 6, 16–19, McGraw-Hill, New York, 2007.
15. Balanis, C. A., *Antenna Theory: Analysis and Design*, 3rd Edition, Chapter 2, Wiley, New York, 2012.
16. CTIA, The Wireless Association, http://www.ctia.org/.
17. Forearm phantom with hand, SPEAG, Schmid & Partner Engineering AG, http://www.speag.com/products/em-phantom/hands/forearm-2/.
18. Sojuyigbe, S. and K. Daniel, "Wearables/IOT devices challenges and solutions to integration of miniature antennas in close proximity to the human body," *IEEE Symposium on Electromagnetic Compatibility and Signal Integrity*, 75–78, Santa Clara, CA, 2015.